THE ASTROPHYSICAL JOURNAL, 325:604–609, 1988 February 15

H_2 AND H I EMISSION LINE IMAGING OF THE RING NEBULA (NGC 6720)

MATTHEW A. GREENHOUSE, THOMAS L. HAYWARD, AND HARLEY A. THRONSON, JR.
Wyoming Infrared Observatory, Department of Physics and Astronomy, University of Wyoming
Received 1987 May 4; accepted 1987 August 13

ABSTRACT

We present infrared emission-line images of the $v = 1 \rightarrow 0$ $S(1)$ transition of molecular hydrogen and Brγ recombination line of atomic hydrogen which cover the entire extent of NGC 6720, the Ring nebula. The maps presented here are the highest angular resolution images of these transitions yet produced for this object and have very low relative positional uncertainty. As a result, we clearly resolve the spatial stratification of the ionized and shocked molecular zones within the nebula. These data, and data from the *Infrared Astronomical Satellite*, are used to determine the H_2, H I, and dust mass within the nebula. Energy sources for the dust heating, formation and destruction of the H_2, and overall evolution of the nebula are also discussed.

Subject headings: infrared: spectra — nebulae: individual (NGC 6720) — nebulae: planetary — radiation mechanisms

I. INTRODUCTION

Approximately 1500 planetary nebulae have been identified to date; however, only roughly 15% of these have sufficient angular extent to allow the distribution of atomic and molecular gas within them to be studied in detail. Most have morphologies in which the optical emission is distributed symmetrically about the stellar remnant. In many cases, this emission is seen to fill a spherical volume, usually with some filamentary structure. In a relatively few cases, the emitting region is confined to an apparent thin spherical shell which gives such nebulae a ringlike appearance on the sky. We plan to study the detailed spatial distribution of H_2, H I, and dust in these nebulae via infrared broad-band and emission-line imagining, in an effort to place the two morphologies in a comparative evolutionary perspective. Here we present first results of our program.

NGC 6720 (the Ring nebula) is a planetary nebula within which the emitting region appears as a thin shell. The spatial distribution of gas in this object has been under study for some 70 yr (e.g., Curtis 1918; Minkowski and Osterbrock 1960; Louise 1974; Atherton *et al.* 1978). The most recent visible emission-line imaging using nonphotographic techniques has been done by Kupferman (1983). Molecular hydrogen emission was discovered in the Ring by Beckwith, Persson, and Gatley (1978) and has been studied recently by Zuckerman and Gatley (1988) who produced a low angular resolution, high-spectral–resolution isophotal contour map of the $v = 1 \rightarrow 0$ $S(1)$ line of H_2 over the whole nebula. Here we report imaging of the same molecular hydrogen line, as well as the Brγ recombination line of atomic hydrogen and near-infrared continuum emission over the entire nebula at twice the spatial resolution, but lower spectral resolution.

II. OBSERVATIONS

A 4 square arcminute region centered on $\alpha(1950) = 18^h51^m43^s.75$, $\delta(1950) = +32°57'56''.2$ corresponding to the approximate center of the visible nebula was imaged during 1985 September 13–14 and 1985 October 17 using the Wyoming Infrared Observatory (WIRO) 234 cm telescope and InSb CVF spectrometer equipped with a DC-coupled integrating amplifier. The radiometer has been described by Hackwell, Grasdalen, and Gehrz (1983). The single-detector imaging and analysis techniques used were similar to those discussed by Castelaz *et al.* (1985) and Grasdalen, Hackwell, and Gehrz (1984). All maps were made using a 10″ FWHM beam, moved in 1″ steps on the sky with a total integration time of 0.1 s per position. The measured resolution of the CVF was $\lambda/\Delta\lambda = 65$. Wavelength calibration of the CVF used Brγ in NGC 7027 and C IV in HD 193793, which are both high-contrast features at this resolution (see, e.g., Smith *et al.* 1981; Lambert and Hinkle 1984).

Each infrared image consists of a mosaic of four 64″ × 64″ images which overlap by 4″. The emission-line maps were made at 2.122 μm and 2.166 μm, corresponding to $v = 1 \rightarrow 0$ $S(1)$ and Brγ transitions of molecular and atomic hydrogen, respectively. Continuum maps were made at 2.26 and 2.29 μm. We detect the continuum with a signal-to-noise ratio greater than 3 over a negligible portion of the area seen in line emission and, hence, use a co-addition of the 2.26 and 2.29 μm continuum images to determine the continuum background at the line wavelength. No continuum emission has been subtracted from the emission-line images.

Both emission lines were imaged over the whole nebula on both observing runs, and the resulting two map sets were co-added. All of the maps have been convolved with a 7″ FWHM Gaussian smoothing function and are displayed in Figure 1 (Plate 21) with a relatively low zero point to illustrate the mosaic boundaries and character of the noise. The 1 σ noise level for all of the images shown is 4.5×10^{-16} ergs s^{-1} cm^{-2} arcsec^{-2}. We estimate the relative positional uncertainty between the quadrants of the mosaics to be $\pm 2''$ in α and $\pm 1''$ in δ.

Surface brightness was measured relative to HD 162208 and α Lyr during September and October, respectively. The absolute flux densities were interpolated from the broad-band magnitudes reported by Elias *et al.* (1982) for HD 162208, and Gehrz, Hackwell, and Jones (1974) for α Lyr. Zero magnitude flux densities were interpolated from the WIRO photometric system described by Gehrz, Grasdalen, and Hackwell (1987) and taken as 710 and 690 Jy at 2.122 and 2.166 μm, respectively. Absolute calibration between the two observing runs was found to agree to within 10%.

The peak brightness of the major emission knots, their offset positions relative to the image center, and the relative and

PLATE 21

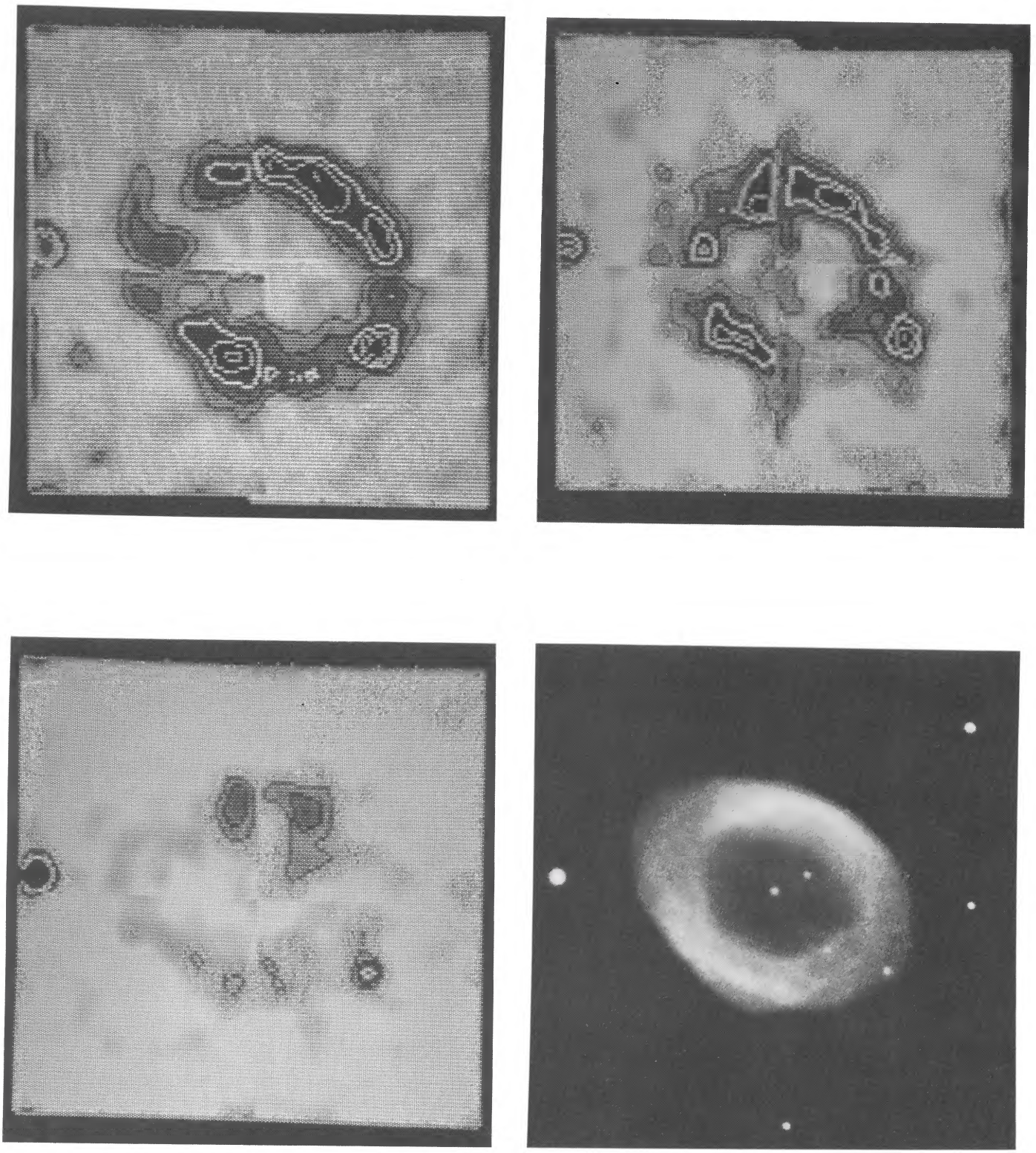

FIG. 1.—The surface brightness distribution of NGC 6720. (*a*) (*upper left*) the $v = 1 \rightarrow 0$ $S(1)$ transition of molecular hydrogen; (*b*) (*upper right*) the Brγ recombination line of atomic hydrogen; (*c*) (*lower left*) 2 μm free-free continuum; and (*d*) (*lower right*) Palomar Observatory photograph taken through a red filter. The counter levels shown are 8.40×10^{-16}, 1.26×10^{-16}, 1.68×10^{-15}, 2.10×10^{-15}, and 2.52×10^{-15} ergs s^{-1} cm^{-2} arcsec^{-2}. The highest two levels are omitted on the continuum map. Each image is 2′ on a side with north up and east to the left in all cases.

TABLE 1

PEAK SURFACE BRIGHTNESS AND POSITION OF EMISSION KNOTS IN NGC 6720

$\Delta\alpha$[a] arcsec ±2	$\Delta\delta$[a] arsec ±1	Flux[b] H I ±0.45	Flux[b] H_2 ±0.45	Note
−15.....	23	2.62		
−27.....	12	2.05		
14.....	−17	2.33		
20.....	5	2.24		
6.....	17	2.44		
2.....	26		2.09	
−6.....	26		2.68	
−19.....	23		2.66	
−35.....	8		2.53	
4.....	−24		2.75	
25.....	5		1.80	
−35.....	−18			Field star
57.....	5			Field star

[a] North, east > 0, offsets relative to
$\alpha = 18^h51^m43^s.75 \pm 0.12$, $\delta = +32°57'56''.2 \pm 1.5$

[b] Units of 10^{-15} ergs s^{-1} cm^{-2} $arcsec^{-2}$, uncorrected for continuum emission.

absolute positional uncertainties are listed in Table 1. Two field stars have been included among these as an aid to determining the absolute position of the peaks. The total brightness of the nebula in each line and the estimated continuum background at each line wavelength is listed in Table 2. A summary of physical properties derived from these data is given in Table 3. The assumed distance to the Ring is 525 pc. This distance is the mean of several published values, and we caution the reader that the distance uncertainty to this and most planetaries is large. We estimate the uncertainty for the value adopted here as ±40%.

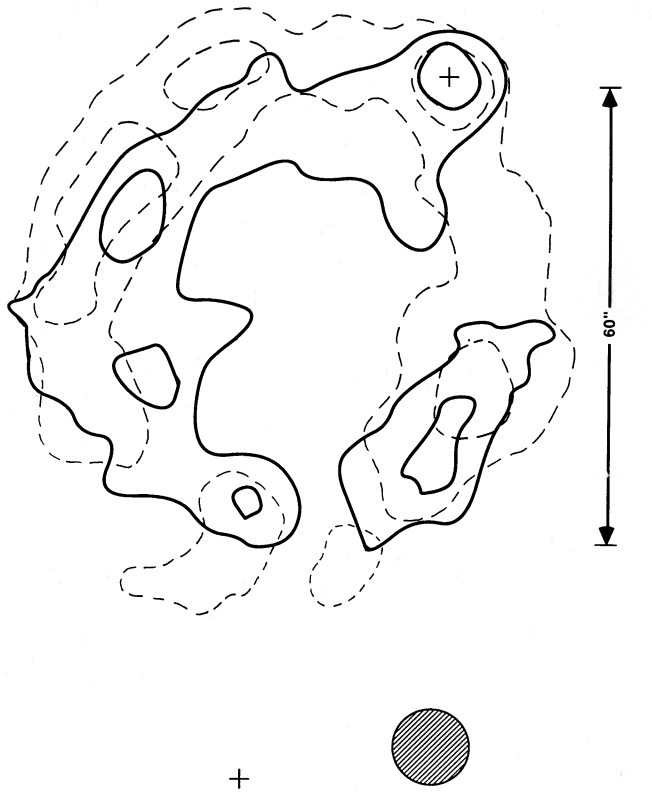

FIG. 2.—The relative spatial distribution of H_2 and H I in NGC 6720 is shown by isophotal contours of emission due to the H_2 $v = 1 \rightarrow 0$ $S(1)$ transition (*dashed*) and H I Brγ recombination line (*solid*). The two contour levels are 1.32×10^{-15} (3 σ) and 2.20×10^{-15} ergs s^{-1} cm^{-2} $arcsec^{-2}$ for both. Crosses denote field stars listed in Table 1. North is up, east is to the left. The relative positional uncertainty between the H_2 and H I maps is ±2″.

III. ANALYSIS

a) *Spatial Distribution of* H_2 *and* H I

The surface brightness distribution of the H_2 and H I lines and 2 μm free-free continuum are shown in Figures 1*a–c* (Plate 21), respectively. The distribution consists of knots embedded in an extended emission which generally follows the optical continuum radiation shown in Figure 1*d*. Most of the line-emission knots are associated with knots of 2 μm continuum emission shown in Figure 1*c*. In addition, the positions of the major Brγ peaks are in good qualitative agreement with the Hβ map produced by Atherton *et al.* (1978). The H_2 emission exhibits a more clumplike distribution than is apparent on the map of Zuckerman and Gatley (1988). This difference is due to the higher angular resolution of the WIRO images, and we expect this trend toward increased clumpy appearance to continue with increasing spatial resolution.

TABLE 2

TOTAL LINE INTENSITIES IN NGC 6720

Transition	λ μm	Flux[a] ±10%	Continuum[a] ±10%	$F_{H_2,HI}$[a] ±10%
$v = 1 \rightarrow 0$ $S(1)$	2.122	7.26	2.10	5.16
Brγ	2.166	5.94	2.10	3.84

[a] Units of 10^{-12} ergs s^{-1} cm^{-2}.

Isophotal contours of the H_2 and H I line emission have been superposed in Figure 2. One finds that in the northern half of the nebula, the H_2 emission lies outside the Brγ emission as previously found by Beckwith, Persson, and Gatley (1978). However, in the southeast quadrant, the emission from the two lines is more coincident, and in much of the southwest quadrant, the Brγ emission is notably reduced at locations of relatively strong H_2 emission. The H_2 and H I maps of this figure were properly registered with respect to each other since (1) the H_2 and Brγ lines were imaged on the same night under identical conditions, (2) the same two field stars are apparent on both line images, and (3) the maps could be shifted with respect to each other within our image processor, to zero small field star offsets, which arise from the finite precision of the telescope pointing. We estimate the registration uncertainty between the two contour maps in Figure 2 to be ±2″.

The reduced Brγ emission we observe in the southern part of the nebula may mark the onset of breakup of the nebular shell due to its ongoing expansion. We feel, as a result of the discussion in § III*f*, that the time development of the H_2–H I stratification seen in the northern half of the nebula is such that the preexisting shocked molecular hydrogen that we observe has been overtaken by an expanding ionization front. The shocked molecular zone is undergoing substantial erosion by the plasma and, to a large extent, presently exists as self-shielded H_2 clumps surrounded by H I recombination envelopes.

TABLE 3

DERIVED PROPERTIES OF NGC 6720

Parameter	Value	Notes
Distance	525 pc	Assumed
E_m	5.9×10^4 cm^{-6} pc	Averaged over H recombination zone
IRE	1.1	Infrared excess ($F_{IR}/F_{Ly\alpha}$)
F_{IR}	3.7×10^{-9} ergs s^{-1} cm^{-2}	Integrated *IRAS* fluxes
L_*	135 $L_\odot$	
L_{IR}	31.7 $L_\odot$	
M_{H_2}	2.7×10^{-6} $M_\odot$	Shocked gas only
M_d	1.2×10^{-3} $M_\odot$	
M_g	3.9×10^{-2} $M_\odot$	Ionized gas only
$N(<912)$	9.5×10^{45} photons s^{-1}	Ionizing photon rate
n_e	600 cm^{-3}	Averaged over H recombination zone
r_*	2.9×10^{-2} $r_\odot$	
T_*	1.17×10^5 K	Pottasch 1984
T_d	50 K	From 60 μm and 100 μm *IRAS* fluxes
T_e	10^4 K	Pottasch 1984

The relative distribution of H_2 and H I shown in Figure 2 is typical of many planetaries which exhibit shocked H_2 emission (e.g., see Zuckerman and Gatley 1988) and is similar to that predicted by the interacting stellar-winds model (ISWM) of planetary nebulae formation. This model is discussed extensively by Kwok, Purton, and FitzGerald (1978), Giuliani (1981), Kahn (1983), Kwok (1983), and Volk and Kwok (1985). Its description will not be repeated here. However, it is interesting to examine our Figure 2 and the schematic diagram of the ISWM appearing in Volk and Kwok. If the outer radii of the H recombination zone (r_H) and the shocked molecular zone (r_{H_2}) expand at approximately the same rate, and if the velocity (v) is known, the observed difference can be used to roughly estimate the lifetime (τ) of the protoplanetary phase as $(r_{H_2} - r_H)v^{-1} \sim \tau$. For the observed difference in the northern half of Figure 2, and $v = 30$ km s^{-1} (Pottasch 1984), we find $\tau \leq 10^3$ yr. The upper limit results from the lack of stratification in the southern part of the nebula. Kwok (1985) argues that an observational upper limit exists on τ for all protoplanetaries such that $\tau < 1500$ yr, which suggests that in the northern half of this nebula, the expansion velocity of the recombination zone v_H has, at most, been only slightly greater than that of the shocked molecular zone v_{H_2} over the lifetime of the expansion.

It is interesting to note that, in general, if $v_H < v_{H_2}$, one would expect nearly all planetary nebulae to exhibit shocked H_2 emission, contrary to observation, and if $v_H > v_{H_2}$, shocked H_2 emission would be apparent only during a small portion of the true planetary nebula phase. In this case, one would expect to find $(r_{H_2} - r_H)r_{H_2}^{-1}$ largest in young planetaries, if they could be spatially resolved at 2 μm. Furthermore, there could exist a time such that $r_H > r_{H_2}$ when we would have direct ionization of the unshocked remnant red-giant wind material (RGWM). Since this relatively cool neutral material is quite likely optically thick shortward of the Lyman limit, one cannot use the absence of shocked H_2 emission as a sufficient condition for assuming that a given nebula is density-bounded. Rather, one should use far-infrared emission from dust within the RGWM for this purpose. Further, if this latter condition is common, perhaps very little unionized RGWM is returned to the interstellar medium.

b) *The* $v = 1 \rightarrow 0$ $S(1)$ *Line of* H_2

In this section we use the total intensity of the H_2 line given in Table 2 to calculate the total observed mass of molecular hydrogen in the nebula. The $v = 1 \rightarrow 0$ $S(1)$ transition requires excitation ($h\nu/k$) of order 10^3 K. This energy can be provided by collisional heating in shock fronts (e.g., see Kwan 1977; and Shull 1982). Alternatively, this emission can be produced through UV fluorescence (e.g., see Black and Dalgarno 1976; Shull 1978; Shull 1982; also Black and Dishoeck 1988). These two processes produce characteristic relative intensities between the various H_2 vibration rotation lines. A K band CVF spectra of the Ring obtained recently by Zuckerman and Gatley (1988) is consistent with shock excitation at $T_{ex} = 2000$ K.

The total line intensity observed at Earth in the optically thin limit is given by

$$F_{1\rightarrow 0\,S(1)} = A_{1\rightarrow 0\,S(1)} h\nu N(v, J) e^{-\tau}/4\pi d^2 \text{ ergs s}^{-1} \text{ cm}^{-2}, \quad (1)$$

where $h\nu$ is the photon energy, $A_{1\rightarrow 0\,S(1)}$ is the spontaneous emission coefficient for the H_2 line, $N(v, J)$ is the number of molecules in the state v, J, d is the distance to the nebula, and τ is the dust optical depth at the line frequency. With $E_{B-V} = 0.07$ (Pottasch 1984), interstellar extinction of the line is negligible; we assume that intranebular extinction is also negligible. Spontaneous emission coefficients for the quadrupole vibration-rotation transitions of H_2 are given by Turner, Kirby-Docken, and Dalgarno (1977), who list $A_{1\rightarrow 0\,S(1)} = 3.47 \times 10^{-7}$ s^{-1}.

Now if the level population is given by a Boltzmann distribution, then

$$N(v, J)/N(H_2) = (2J + 1) g_s Q(T_{ex})^{-1} \exp(-h\nu/kT_{ex}), \quad (2)$$

where $Q(T_{ex})$ is the total molecular internal partition function, g_s is the spin statistical weight, T_{ex} is the excitation temperature, and $N(H_2)$ is the total number of shocked H_2 molecules. Calculation of the partition function for a variety of diatomic molecules has been discussed recently by Sauval and Tatum (1984). They find that for H_2, $Q(2000) = 2.19$. Taking the total line intensity $F_{1\rightarrow 0\,S(1)}$ from Table 2, we find $N(H_2) = 1.6 \times 10^{51}$ or $M(H_2) = 2.7 \times 10^{-6}$ $M_\odot$. For comparison, the mass of shocked H_2 seen here is in agreement with the H_2 mass calculated for the Ring by Zuckerman and Gatley (1988); however, it is two to three orders of magnitude less than that observed in younger planetaries (e.g., see Thronson 1981; Smith, Larson, and Fink 1981). This difference is interpreted in § III*f*.

c) *The* Brγ *Recombination Line*

Here we use the total Brγ line flux to derive an emission measure, ionizing photon rate, and mass for the H recombination zone in the nebula. We then use these to calculate the effective radius and luminosity of the central star. It is first necessary to assess the optical depth of the nebula in the H Lyman continuum which we do by the following method.

The optical depth in the He Lyman continuum is

$$\tau(<229) = \kappa(<229) n_e r_n n(\text{He II})/n(\text{H II} + \text{H I}) , \quad (3)$$

where $\kappa(<229)$ is the absorption coefficient for $\lambda < 229$ Å, and r_n is a characteristic path length through the nebula. We take $n(\text{He II})/n(\text{H II} + \text{H I}) \sim 0.10$, $\kappa(<229) = 1.7 \times 10^{-18}$ cm^2 (Pottasch 1984), $n_e \sim 600$ cm^{-3}, and $r_n = 2.5 \times 10^{17}$ cm at the assumed distance, and find that $\tau(<229) \sim 26$ so that the nebula is unambiguously optically thick for $\lambda < 229$ Å.

Helium and hydrogen Zanstra temperature (T_Z) determinations for the central star assume, respectively, that the nebula is optically thick at the helium and hydrogen Lyman continuum (e.g., see Seaton 1975; Natta, Pottasch, and Preite-Martinez 1980). If these two temperature calculations are in close agreement, and the stellar remnant emits as a blackbody, one can deduce that the nebula is optically thick shortward of 912 Å (although the converse is not true). This object has T_Z(He) and T_Z(H) reported as 100 and 117 $\times 10^3$ K, respectively (Pottasch 1984). Hence, we take coefficients appropriate for case B emission in evaluating the recombination line data.

The specific intensity of the Brγ line is given by

$$I = \int j_{\text{Br}\gamma}\, ds$$

$$= 3.05 \times 10^{-8} \frac{j_{\text{Br}\gamma}}{j_{\text{H}\epsilon}} \frac{j_{\text{H}\epsilon}}{j_{\text{H}\beta}} E_m \text{ ergs}^{-1} \text{ cm}^{-2} \text{ sr}^{-1} , \quad (4)$$

where E_m is the emission measure in units of cm^{-6} pc, and the j's are the volume emission coefficients for Brγ, Hϵ, and Hβ emission. We wish to calculate an emission measure averaged over the H recombination zone as a whole and, hence, take $I = F_{\text{Br}\gamma}/\Omega$ where $F_{\text{Br}\gamma}$ is the total intensity of the Brγ line from Table 2, and $\Omega = 7.74 \times 10^{-8}$ sr is the solid angle subtended by the area seen in Brγ emission. We have assumed that the emission coefficients and electron density are independent of position within the nebular shell which is reasonable since these coefficients are weakly dependent on temperature. We use $j_{\text{H}\epsilon}/j_{\text{H}\beta} = 0.159$ (Osterbrock 1974), $j_{\text{Br}\gamma}/j_{\text{H}\epsilon} = 0.174$ (Giles 1977), and $T_e = 10^4$ K (Kupferman 1983; Pottasch 1984), and find $E_m = 5.9 \times 10^4$ cm^{-6} pc averaged over the region seen in Brγ emission. This emission measure implies an rms electron density of 600 cm^{-3} which is in good agreement with most other density determinations from optical recombination line studies (e.g., see Pottasch 1984). In addition, some rough stellar parameters can be derived from the recombination line data under the assumption that each ionizing photon emitted by the star is balanced by a recombination of H, consistent with our assumption that the nebula is ionization bounded.

The photon rate shortward of $\lambda = 912$ Å as measured by the Brγ line is

$$N(<912) = 4\pi d^2 F_{\text{Br}\gamma} (h\nu)^{-1} \alpha_B^{\text{eff}}/\alpha_{\text{Br}\gamma}^{\text{eff}} \text{ photon s}^{-1} , \quad (5)$$

where d is the distance of the nebula, α_B^{eff} is the total effective recombination rate coefficient to all levels except $n = 1$, and $\alpha_{\text{Br}\gamma}^{\text{eff}}$ is the effective recombination rate coefficient for the Brγ transition. We can write $\alpha_{\text{Br}\gamma}^{\text{eff}} = \alpha_{\text{H}\beta}^{\text{eff}} (j_{\text{Br}\gamma}/j_{\text{H}\beta})(\nu_{\text{H}\beta}/\nu_{\text{Br}\gamma}) = 0.122 \alpha_{\text{H}\beta}^{\text{eff}}$ where $\alpha_{\text{H}\beta}^{\text{eff}} = 3.03 \times 10^{-14}$ cm^3 s^{-1} and $\alpha_B^{\text{eff}} = 2.6 \times 10^{-13}$ cm^3 s^{-1} (Osterbrock 1974). We then find $N(<912) = 9.5 \times 10^{45}$ photons s^{-1}.

Now, we also have that $N(<912) = \int_{\nu_0}^{\infty} L_\nu/h\nu\, d\nu$ where L_ν, the luminosity of the star, is $4\pi^2 r_*^2 B_\nu(T_*)$, where $\nu_0 = 3.29 \times 10^{15}$ Hz, $T_* = 1.17 \times 10^5$ K is the effective stellar temperature, and r_* is the effective stellar radius. We find $r_*/r_\odot = 2.9 \times 10^{-2}$ which implies a total luminosity of $L_*/L_\odot = (r_*/r_\odot)^2 (T_*/T_\odot)^4 = 135$. We note that B_ν may be an inappropriate source function for the stellar radiation shortward of 912 Å. However, the luminosity calculated here under the blackbody assumption is in good agreement with other data (Pottasch 1984), and the effective stellar radius seems quite reasonable compared to white dwarfs in general (Allen 1973).

Schonberner (1983) has modeled the evolution of low-mass asymptotic giant branch (AGB) stars into the central stars of planetary nebula. The present effective temperature and luminosity of the Ring central star lie on the evolutionary track of a one solar mass AGB star (see Schonberner's Fig. 2). The model suggests that approximately 4×10^4 yr have elapsed since cessation of the high-velocity mass loss predicted by the interacting stellar-winds model, and that the stellar remnant has now settled onto the white dwarf cooling track.

Finally, we can estimate the total mass of ionized gas in the nebula as

$$M_g = (1.6 \times 10^{-24}) V n_e (1 + 4\text{He/H}) \text{ g} , \quad (6)$$

where n_e is the measured rms electron density, and $V = 5.6 \times 10^{51}$ cm^3 is the annular volume of the region seen in Brγ emission. We take He/H as 0.11 (Osterbrock 1974) and find that $M_g = 3.9 \times 10^{-2}\, M_\odot$, in agreement with the empirical correlation between ionized gas mass and radius of the ionized zone found for many planetaries (Volk and Kwok 1985 and references therein).

e) *The Dust*

The formation of H_2 in the nebula may be catalyzed by dust, and the ultimate survival of the molecules is probably influenced in an important way by the spatial distribution and opacity of the dust to the ionizing radiation. Although attempts to map the dust distribution in the N and Q bands have been unsuccessful to date, some information can be derived from data collected by the *Infrared Astronomical Satellite* (*IRAS*).

The *IRAS* spectrum is shown in Figure 3 along with modified Planck source functions of the form $\nu^n B_\nu$ for $n = 0$ and 1. The observed distribution cannot be described by an isothermal dust model and probably represents the envelope of a series of source functions corresponding to dust temperatures in the range of 50–150 K. The interpretation shown in Figure 3 is, of course, not unique with respect to the choice of $n = 1$. It is possible that the shell is not well-mixed, resulting in spatial stratification of the grains with respect to composition. If large compositional gradients exist in the dust, then n becomes a function of position. Nonetheless, we take $n = 1$ as a working hypothesis, and adopt a single dust temperature, $T_d = 50$ K derived from the 60–100 μm flux density ratio for subsequent calculations.

The total mass of the dust in the nebula can be estimated in a standard way from these data as follows. Consider grains of radius a, emissivity Q_ν, mass density ρ, and number density n_d contained in a nebula of radius r_n. The flux density from the

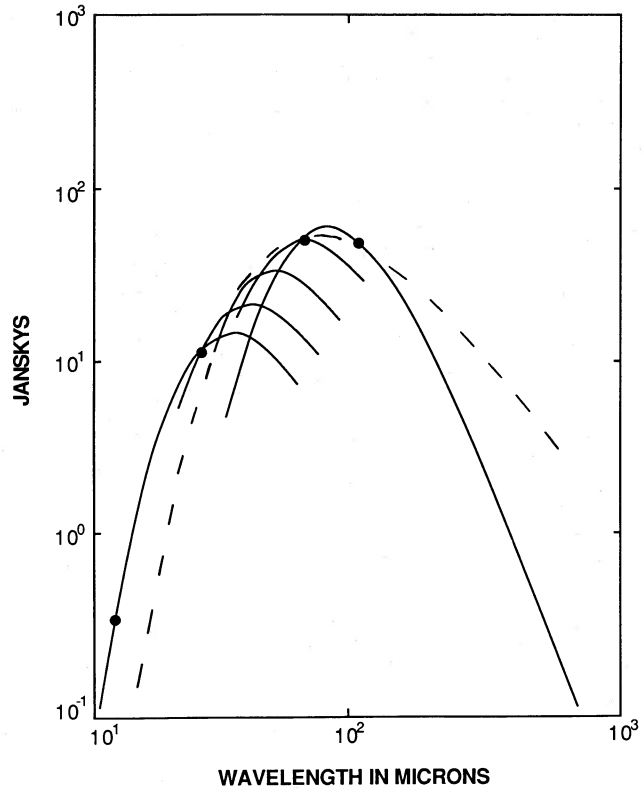

FIG. 3.—The *IRAS* color-corrected flux densities and source functions of the form $\nu^n B_\nu$ for $n = 0$ (*dashed*) and $n = 1$ (*solid*).

dust is then $4\pi d^2 F_\nu = (4\pi r_n^3/3)4\pi a^2 n_d Q_\nu \pi B_\nu(T_d)$ ergs s^{-1} Hz^{-1} while the mass of dust in the nebula is simply $M_d = (4\pi r_n^3/3)(4\pi a^3/3) n_d \rho$. Eliminating n_d then gives M_d in terms of F_ν as $M_d = (4a\rho/3Q_\nu) d^2 F_\nu / B_\nu(T_d)$. We take $4a\rho/3Q_\nu = 4 \times 10^{-2}$ g cm^{-2} (Hildebrand 1983) and find that

$$M_d = 4.82 \times 10^{-12} d^2 F_\nu [\exp(144/T_d) - 1]\ M_\odot \qquad (7)$$

for F_ν in Jy and d in parsecs. Taking $F_{\nu,\max} = 55$ Jy we find that $M_d = 1.2 \times 10^{-3}\ M_\odot$. The expanding nebula has displaced a volume sufficient to sweep up only $10^{-6}\ M_\odot$ of dust assuming an interstellar density of matter in dust grains of 1.8×10^{-26} g cm^{-3} (Spitzer 1978). Hence, the observed dust was formed either within the nebula or primordially by the precursor star.

What heats the dust? The two primary sources of energy input into the dust are absorption of direct stellar radiation and diffuse line radiation to which the nebula is optically thick. The latter can dominate, since such photons migrate through the nebular shell in a random walk process, developing an enormous effective path length and, hence, a high probability of being absorbed by dust. We can assess the extent to which diffuse trapped Lyα photons are important in driving the dust luminosity as follows. The infrared excess (IRE) is defined as IRE $= F_{\rm IR}/F_{\rm Ly\alpha}$ which can be written as

$$\mathrm{IRE} = \frac{F_{\rm IR}}{F_{\rm Br\gamma}} \frac{I_{\rm Br\gamma}}{I_{\rm Ly\alpha}}, \qquad (8)$$

where $F_{\rm IR}$ is the total integrated infrared flux derived from the *IRAS* data, and $I_{\rm Br\gamma}/I_{\rm Ly\alpha} = (\nu_{\rm Br\gamma}/\nu_{\rm Ly\alpha})\alpha_{\rm Br\gamma}^{\rm eff}(\alpha_B^{\rm eff} - \alpha_{2^2s}^{\rm eff})^{-1} = 1.18 \times 10^{-3}$ where $\alpha_{2^2s}^{\rm eff} = 0.838 \times 10^{-13}$ cm^3 s^{-1} (Osterbrock 1974) is the total effective recombination rate coefficient for the two quantum process. Integrating the *IRAS* spectrum shown in Figure 3 using νB_ν to extrapolate beyond 100 μm, we find $F_{\rm IR} = 3.7 \times 10^{-9}$ ergs s^{-1} cm^{-2} and, hence, find an IRE of 1.1 for the nebula. An IRE ≤ 1 suggests that the diffuse Lyα field is a sufficient energy source for the observed mid- and far-infrared luminosity. Hence, direct stellar radiation and other trapped line radiation make only a very small contribution to the dust energetics in the Ring.

f) *Formation and Destruction of the* H_2

Is the observed H_2 undergoing net formation or destruction? Molecular hydrogen in low-density planetary nebulae is primarily destroyed by photodissociation. We use equation (5-47) of Spitzer (1978) to describe a steady-state condition between formation and photodissociation of H_2,

$$n(\mathrm{H\ I})/n(\mathrm{H_2}) = \langle k \rangle \beta_0 / R n(\mathrm{H}), \qquad (9)$$

where β_0 is the rate of photoabsorption for the molecules in the Lyman and Werner bands, $\langle k \rangle$ is the probability that an absorption results in dissociation, R is the H_2 formation constant and $n(\mathrm{H}) = n(\mathrm{H\ I} + \mathrm{H\ II})$. The ionization equilibrium at the location of the H_2 is

$$\frac{n(\mathrm{H\ II})}{n(\mathrm{H\ I})} = \frac{r_*^2}{r_n^2 n_e \alpha_b^{\rm eff}} \int \frac{\sigma_\nu \pi B_\nu}{h\nu}\, d\nu \sim (6 \times 10^{-18}) \times \frac{r_*^2}{r_n^2 n_e \alpha_B^{\rm eff}} \int \frac{\pi B_\nu}{h\nu}\, d\nu \sim 4 \times 10^3 \qquad (10)$$

where σ_ν is the photoionization cross section for H.

Now $\langle k \rangle$ is of order 10^{-1}, while R is of order 10^{-17} cm^3 s^{-1} (Spitzer 1978). A minimum value for β_0 is that applicable to the interstellar medium, 10^{-10} s^{-1} (Jura 1974). Hence, taking $n(\mathrm{H}) \sim n_e$, and $n(\mathrm{H\ I}) \sim n_e/4 \times 10^3$ we find $n(\mathrm{H\ I})/n(\mathrm{H_2}) \sim 10$ compared to the steady-state ratio given by equation (9) of at least 10^3. This result suggests that the observed H_2 is in excess of that which could form in place under the present ionization conditions within the nebula. It would appear that the H_2 formed in a zone outside the advancing ionization front and has been overtaken by it. Some molecules may survive within the recombination zone by virtue of self-shielding and the opacity of dust clumps which may be present. However, it seems clear that the nebula is undergoing a period of net H_2 dissociation—consistent with the low observed H_2 mass relative to younger planetaries (§ III*b*).

IV. CONCLUSIONS

The H_2 and H I emission is spatially stratified in the northern half of the nebula and coincident in the southern half. The shocked molecular zone traced by the observed H_2 emission is being overtaken by an advancing ionization front, and the nebula is undergoing a period of net H_2 dissociation as a result. The Ring nebula is seen by *IRAS* to contain relatively cool dust. However, its spatial distribution and relation to the molecular hydrogen is as yet unknown. Since this dust may play a critical role in the early formation of H_2, and since its emission may trace the boundary between the RGWM and the shocked H_2, infrared images which illustrate the detailed spatial distribution of H_2, H I, and dust in planetaries at several stages of evolution are crucial to understanding the general evolution of such objects.

The next generation of seeing-limited infrared cameras under development at WIRO and elsewhere for use in the *K* and *N* bands will make younger, more compact planetaries

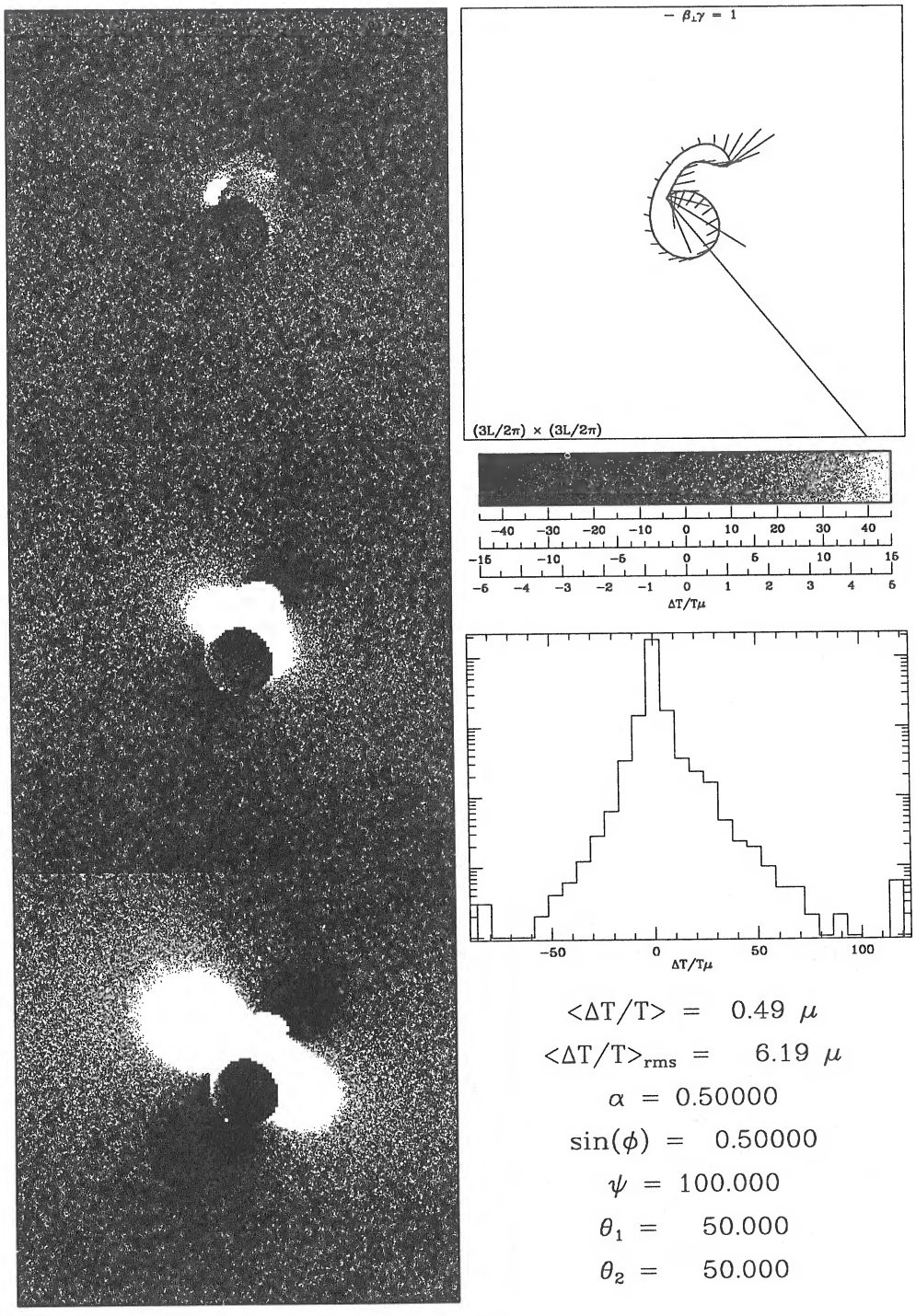

FIG. 4*f*